

Person Re-identification in the 3D Space

Zhedong Zheng, Yi Yang

University of Technology Sydney, Australia

zhedong.zheng@student.uts.edu.au, yi.yang@uts.edu.au

Abstract

People live in a 3D world. However, existing works on person re-identification (re-id) mostly consider the representation learning in a 2D space, intrinsically limiting the understanding of people. In this work, we address this limitation by exploring the prior knowledge of the 3D body structure. Specifically, we project 2D images to a 3D space and introduce a novel Omni-scale Graph Network (OG-Net) to learn the representation from sparse 3D points. With the help of 3D geometry information, we can learn a new type of deep re-id feature free from noisy variants, such as scale and viewpoint. To our knowledge, we are among the first attempts to conduct person re-identification in the 3D space. Extensive experiments show that the proposed method achieves competitive results on three popular large-scale person re-id datasets, and has good scalability to unseen datasets. The code is available at ¹.

1 Introduction

Person re-identification is usually regarded as an image retrieval problem of spotting the person in the non-overlapping cameras [43, 46]. The main challenge is to learn the robust person representation against appearance variants due to the viewpoint changes. In recent years, many researchers and companies have pushed the model performance, and claimed that the model surpasses human performance [38, 44]. However, one scientific problem still remains: does the model really understand the person? We notice that most prevailing person re-id methods ignore the prior knowledge that human is a 3D non-rigid object, and only focus on learning the representation in 2D space. For instance, one of the existing works, PersonX [24], has applied the game engine to build 3D person models. However, representation learning is still conducted in the 2D space by projecting the 3D model back to 2D images. This line of works is effective but might be sub-optimal. It is because the 2D data space intrinsically limits the model to learn the 3D geometry information of the person.

In this paper, we argue that the key to learning an effective and scalable person representation is to consider both the human appearance and 3D geometry structure. With the prior knowledge of 3D human geometry information, we could learn a depth-aware model, thus making the representation robust to real-world scenarios. As shown in Figure 1, we map the visible surface to the human mesh, and make the person free from the 2D space. Without the need to worry about the part matching from two different viewpoints, the 3D data structure eases the matching difficulty in nature. The model could concentrate on learning the identity-related features, and dealing with the other variants, such as illumination.

To fully take advantage of the 3D structure and 2D appearance, we propose a novel Omni-scale Graph Network for person re-id in the 3D space, called OG-Net. The model is based on graph neural network (GNN) to communicate between the discrete cloud points of arbitrary locations. In particular, following the spirit of the conventional convolutional neural network (CNN), we adopt the KNN-Graph [30] to capture the information from neighbor points. To leverage multi-scale

¹<https://github.com/layumi/person-reid-3d>

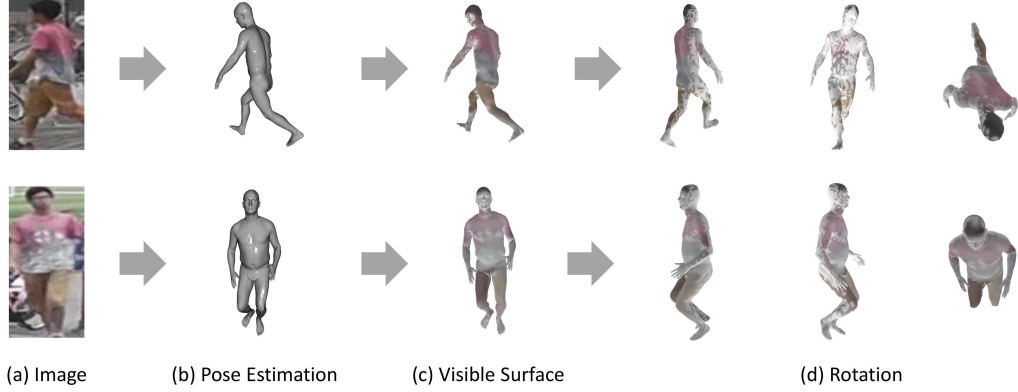


Figure 1: Person is a 3D non-rigid objective. In this work, we conduct the person re-identification in the 3D space, and learn a new type of robust re-id feature. Given one 2D image (a), we first (b) estimate the 3D pose via the off-the-shelf model [10], followed by (c) mapping the RGB color of visible surfaces to corresponding points. The invisible parts are made transparent for visualization. (d) In this work, we make the person free from the 2D space, and thus ease the matching difficulty.

information in 3D data, we propose the Omni-scale module to aggregate the feature from multiple 3D receptive fields. Given the 3D point cloud and the corresponding color information, OG-Net predicts the person identity and outputs the robust human representation for subsequent matching.

Contribution. Our contributions are as follows. (1) We study the person re-identification in the 3D space - a realistic scenario which could better reflect the nature of the 3D non-rigid human. To our knowledge, this work is among the early attempts to address this problem. (2) We propose a novel Omni-scale Graph Network to learn the feature from both human appearance and 3D geometry structure. OG-Net could leverage discrete 3D points to capture the multi-scale identity information. Extensive experiments show the proposed method could achieve competitive performance with limited parameters. A more realistic transfer learning is also studied in this paper. We observe that OG-Net has good scalability to the unseen person re-id dataset.

2 Related work

In this section, we introduce relevant works on person re-identification and point cloud classification.

Person Re-identification. The recent advances in person re-id task focus on two aspects: (1) generating more data to address the data limitation, and (2) mining the local parts to learn discriminative features. In particular, one line of existing works leverages the generative adversarial network (GAN) to synthesize more high-quality training data, and let the model “see” more appearance variants to learn robust representation [44, 3, 2, 18, 45, 12, 48]. Similarly, some works [24, 27, 36] apply the game engine to build 3D models, and project the model to 2D plane for generating 2D training data. In contrast, more researchers focus on the part matching in different levels, such as pixel level [9, 41, 47, 22], and feature level [23, 25, 40, 17, 49]. The discriminative feature could be obtained via mining local patterns. However, the above-mentioned studies are mostly investigated in the 2D space, and neglect the 3D geometry information of human bodies. In this work, we argue that the 3D space with the geometry knowledge could help to learn a new type of feature free from the visual variants, such as viewpoints.

Point Cloud Classification. The point cloud is a flexible geometric representation of 3D data structure, which could be obtained by most 3D data acquisition devices, such as radar. The point cloud data is usually unordered, and thus the conventional convolutional neural network (CNN) could not directly work on this kind of data. One of the earliest works, *i.e.*, PointNet [15], proposes to leverage the multi-layer perceptron (MLP) networks and max-pooling layer to fuse the information from multiple points. PointNet++ [16] takes one more step by introducing the sampling layer to distill salient points. However, the communication between the points is limited, and each point is

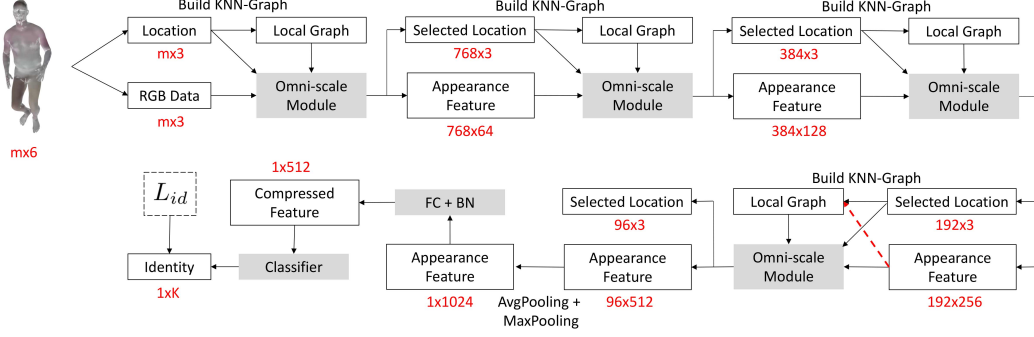


Figure 2: **OG-Net Architecture.** OG-Net is simply built via stacking Omni-scale Modules. $(m' \times c)$ denotes the feature of m' points with c -dim attribute. Given the point cloud of $(m \times 6)$, we split the geometry location and the rgb color data. The 3D location information, *i.e.*, (x, y, z) , is to build the KNN graph, while the rgb data is to extract the appearance feature as the conventional 2D CNNs. We progressively downsample the number of selected points $\{m, 768, 384, 192, 96\}$, while increasing the appearance feature length $\{3, 64, 128, 256, 512\}$. For the last KNN Graph, we concatenate the position and the appearance feature to yield a non-local attention (see the red dash arrow). Finally, we concatenate the outputs of average pooling and max pooling layer, followed by one fully connected (FC) layer and one batch normalization (BN) layer. We adopt the conventional pretext task, *i.e.*, identity classification, as the optimization objective to learn the pedestrian representation.

treated most of the time independently. Therefore, Wang *et al.* [30] propose to leverage Graph Neural Network (GNN) [21] to enable the information spread between the k -nearest points. Similarly, in this work, we regard every person as one individual graph, while every RGB pixel and the corresponding location is viewed as one node in the graph. More details are provided in Section 3.

3 Method

Preliminaries and Notations. Given one person re-id dataset, we first map 2D images to the 3D space via the off-the-shelf 3D pose estimation [10]. We denote the point sets and identity labels as $S = \{s_n\}_{n=1}^N$ and $Y = \{y_n\}_{n=1}^N$, where N is the number of samples in the dataset, $y_n \in [1, K]$, and K is the number of the identity categories. We utilize the matrix format to illustrate the point cloud $s_n \in \mathbb{R}^{m \times 6}$, where m is the number of points, and 6 is the channel number. The former 3 channels contain 3D coordinates XYZ, while the latter 3 channels contain the corresponding RGB information. Given one 3D data $s_n \in \mathbb{R}^{m \times 6}$, we intend to learn a mapping function F which projects the input s_n to the identity-aware representation $f_n = F_\Theta(s_n)$ with learnable parameters Θ .

Dynamic Graph Convolution. In the spirit of the traditional 2D CNN, we deploy one local convolution layer based on the adaptive position, *i.e.*, dynamic graph. Specifically, we adopt the k -nearest neighbor graph $\mathcal{G} = (\mathcal{V}, \mathcal{E})$, where \mathcal{V} denotes the vertex set, and \mathcal{E} denotes the edge set ($\mathcal{E} \subseteq \mathcal{V} \times \mathcal{V}$). The graph is directed, and includes self-loop, meaning $(i, i) \in \mathcal{E}$. Given one node feature x_i , the output x'_i of the dynamic graph convolution could be formulated as:

$$x'_i = \sum_{j: (i, j) \in \mathcal{E}, j \neq i} h(x_i, x_j) = \sum_{j: (i, j) \in \mathcal{E}, j \neq i} (\theta_i x_i + \theta_j x_j) \quad (1)$$

where x_j is the feature of neighbor points in the graph, and there is one edge from i to j . θ is the learnable parameter in Θ . The main difference with the traditional convolution is the definition of the neighbor set. **In this work, we combine two kinds of neighbor choices, *i.e.*, position similarity and feature similarity.** If the graph \mathcal{G} is based on the 3D coordinate similarity, dynamic graph convolution equals to the conventional 2D CNN to capture the local pattern based on the position. We note that this operation is translation invariant, since the global translation, such as ShiftX, ShiftY and Rotation, could not change the local neighbors in \mathcal{E} . On the other hand, if the graph \mathcal{G} is built on the appearance feature, the dynamic graph convolution works as the non-local self-attention as [29, 37], which ignores the local position but pays attention to similar appearance features.

Omni-scale Module. To leverage the rich multi-scale information as the prevailing 2D CNNs, we propose one basic Omni-scale module, which could be easily stacked to form the whole network. The module treats the 3D location and the RGB input differently (see Figure 3). We denote $l \in [0, L - 1]$ as the layer index. The RGB input is the first appearance feature a_0 of $m \times 3$, while the initial 3D position is b_0 of $m \times 3$. Different from the conventional graph CNN, the local k -nearest graph \mathcal{G}_l is dynamically generated according to the input location b_l or the concatenation of a_l and b_l . Given the appearance feature a_l of $m' \times c$, the location b_l of $m' \times 3$ and the KNN graph \mathcal{G}_l , the Omni-scale module outputs the appearance feature a_{l+1} and the selected locations b_{l+1} . From the top to the bottom of the module, we first apply Dynamic Graph Convolution to aggregate the k -nearest neighbor features, which is similar to the conventional convolutional layer. Dynamic Graph Convolution does not change the number of points, and thus the shape of the output feature is $m' \times c'$. Generally, we set $c' = 2c$ to enlarge the feature channel before downsampling. Then we downsample the location according to the farthest point sampling (FPS) [16]. FPS selects the most distinguish points in the 3D space. We note that only the 3D position b_l is used to calculate the distance and decide the selected points when downsampling. According to the selected location, we also downsample the appearance feature, and only keep the feature of the selected location. Therefore, the shape of the selected location is $\frac{1}{2}m' \times 3$, while the selected feature shape is $\frac{1}{2}m' \times c'$. Next we deploy three branches with different grouping rates $r = \{8, 16, 32\}$, and the three branches do not share weights. In this way, we could capture the information with different receptive fields as the conventional 2D CNNs, *i.e.*, InceptionNet [26]. Each branch consists of one grouping layer, two linear layers, two batch normalization (BN) layers, one squeeze-excitation (SE) block [7] and one group max pooling layer to aggregate the local information. Specifically, grouping- r layer is to sample and duplicate the r nearest points for each point, followed by the linear layers, batch normalization and the SE block. We introduce SE-block [7] as one adaptive gate function to re-scale the weight of each branch $x' = x \times \text{sigmod}(h(x))$ before the summarization of three branches. Group max pooling layer is to maximize the feature within each group, *i.e.*, $\max h(x_i)$. Finally, we adopt the ‘add’ to calculate the sum of three branches rather than concatenation, so that the different scale pattern of the same part, such as cloth logos, could be accumulated. The shape of the new appearance feature a_{l+1} is $\frac{1}{2}m' \times c'$, and the shape of the corresponding 3D position b_{l+1} is $\frac{1}{2}m' \times 3$. Alternatively, we could add the short-cut connection to take advantage of the identity representation as ResNet [6].

To summarize, the key of Omni-scale Module is two cross-point functions. The cross-point function indicates the function considers the neighbor points, while the pre-point function only considers the feature of one point itself. One cross-point function is the dynamic graph convolution before downsampling, which could be simply formulated as $\sum h(x_i, x_j)$. It mimics the conventional 2D CNN to aggregate the local patterns according to the position. The other is the max group pooling layer in each branch, which could be simply formulated as $\max h(x_i)$. It maximizes neighbor features in each group as the new point feature.

OG-Net Architecture. The structure of OG-Net is as shown in Figure 2, consisting four Omni-scale modules. We progressively decrease the number of selected points as the conventional CNN. Every time the point number decreases, the channel number of the appearance feature is doubled. After four Omni-scale modules, we could obtain 96 points with 512-dim appearance feature. Similar to [30], we apply the max pooling as well as average pooling to aggregate the point feature, and concatenate the two outputs, yielding the 1024-dim feature. We add one fully-connected layer and one batch normalization layer to compress the feature to 512 dimensions as the pedestrian representation.

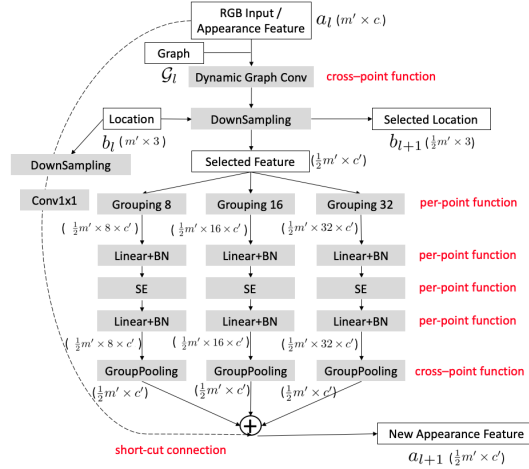


Figure 3: Visualization of Omni-scale Module. We provide the feature shape as the format of (\cdot) . For instance, $(m' \times c)$ denotes the feature of m' points with c -dim attribute. The dash line denotes the short-cut connection. Besides, we highlight cross-point functions and per-point functions.

When inference, we drop the last linear classifier for the pretext classification task, and extract the 512-dim feature to conduct image matching.

Training Objective. We adopt the conventional identity classification as the pretext task to learn the identity-aware feature. The vanilla cross-entropy loss could be formulated as:

$$L_{id} = \mathbb{E}[-\log(p(y_n|s_n))] \quad (2)$$

where $p(y_n|s_n)$ is the predicted possibility of s_n belonging to the ground-truth class y_n . The training objective demands that the model could discriminate different identities according to the input points.

Relation to Existing Methods. The main difference with existing GNN-based networks [30, 35] is three-fold: (1) We extract the multi-scale local information via the proposed Omni-scale Block, which can deal with the common scale variants in 3D person data; (2) We split the XYZ position information and RGB color information, and treat them differently. RGB inputs are used to extract appearance features, while the geometry position is to build the graph for local representation learning; (3) Due to a large number of points in 3D person, we progressively reduce the number of nodes in the graph, facilitating efficient training for 3D person data. On the other hand, compared with PointNet [15] and PointNet++ [16], the proposed OG-Net contains more cross-point functions, and provides topology information, enriching the representation power of the network. The graph could be built on the two kinds of neighbor choices, *i.e.*, position similarity or feature similarity.

4 Experiment

Implementation Details. OG-Net is trained from scratch with a mini-batch of 8. We deploy Adam optimizer [11] and the initial learning rate is set to $3.5e-4$. We gradually decrease the learning rate via the cosine policy [13], and the model is trained for 150 epochs. To regularize the training, we transfer some traditional 2D data augmentation methods, such as random scale and position jittering, to the 3D space. For instance, position jittering is to add zero-mean Gaussian noise to every point. Following the setting in DGCNN [30], we set the neighbor number of KNN-graph to $k = 20$. The dynamic graph convolution in OG-Net can be any of the existing graph convolution operations, such as EdgeConv [30], SAGE [4] and GAT [34]. In practise, we adopt EdgeConv [30]. Dropout with 0.7 drop probability is used before the last linear classification layer. Since the basic OG-Net is shallow, we do not use the short-cut connection. For the person re-id task, the input image size is 128×64 . We uniformly sample the half points to train the OG-Net, and thus the number of input m in Figure 2 is set to 4096. The channel number of the four Omni-scale Module in OG-Net is {64, 128, 256, 512}. To compare with mobile models, we also introduce OG-Net-Small with limited channel numbers, *i.e.*, {48, 96, 192, 384}. The whole training process costs about 20 hours, with one NVIDIA 2080Ti.

Datasets. We verify the effectiveness of the proposed method on three large-scale person re-id datasets, *i.e.*, Market-1501 [42], DukeMTMC-reID [19, 45], and MSMT-17 [31]. Market-1501 is collected in a university campus by 6 cameras, containing 12,936 training images of 751 identities, 3,368 query images and 19,732 gallery images of the other 750 identities. There are no overlapping identities (classes) between the training and test set. DukeMTMC-reID consists 16,522 training images of 702 identities, 2,228 query images of the other 702 identities and 17,661 gallery images, which is mostly collected in winter by eight high-resolution cameras. MSMT-17 is one of the largest datasets, including 126,441 images collected in both indoor and outdoor scenarios. **Evaluation Metrics.** We report Rank-1 accuracy ($R@1$) and mean average precision (mAP). Rank- i denotes the probability of the true match in the top- i of the retrieval results, while AP denotes the area under the Precision-Recall curve. The mean of the average precision (mAP) for all query images reflects the precision and recall rate of the retrieval performance. Besides, we also provide the number of model parameters (#params) and Multiplier-ACcumulator (MAC) for the efficiency comparison.

4.1 Data Limitation

Before the experimental analysis, we would like to illustrate several data limitations. It is mainly due to lossy mapping in the 2D-to-3D process. Due to the restriction of the 3D human model, we could not build the 3D model for several body outliers, such as hair, bag, dress. However, these outliers contain discriminative identity information. For instance, as shown in Figure 4 (a) and (b), the 3D model based on the visible part drops some part of hair and dress of the girl, which is not

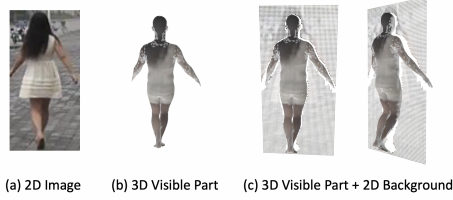


Figure 4: **(a,b)** Visualization of lossy compression in the 2D-to-3D mapping, which drops the body outliers, *e.g.*, hair and dress. **(c)** We still introduce the 2D background to 3D space.

Inputs	R@1	mAP
2D Image [†]	79.13	57.28
3D Visible Part	71.85	48.55
3D Visible Part + 2D Background	80.94	59.97

Table 1: Ablation study of different inputs on Market-1501. [†]: 2D Images are trained with extra 3D coordinates $(x, y, 0)$.

Method	Pre-trained w/ ImageNet [1]	#params(M)	MAC(G)	Market-1501		DukeMTMC-reID		MSMT-17	
				R@1	mAP	R@1	mAP	R@1	mAP
ResNet-50 [6]	✓	24.56	4.08	90.74	77.28	82.45	66.90	59.69	32.66
ResNet-50 [6]	×	24.56	4.08	84.59	65.31	73.20	55.96	46.88	22.25
DenseNet-121 [8]	×	8.50	1.88	83.14	63.36	73.16	55.08	46.32	21.50
ShuffleNetV2 [39]	×	1.78	0.10	79.75	56.80	68.81	48.09	36.80	15.70
MobileNetV2 [20]	×	4.16	0.21	81.95	59.28	71.05	50.45	42.53	18.62
PointNet++ (SSG) [16]	×	1.59	1.08	61.79	37.89	55.70	35.16	22.94	9.61
PointNet++ (MSG) [16]	×	1.87	4.03	72.51	47.21	60.23	39.36	28.99	12.52
DGCNN [30]	×	1.37	15.35	28.89	13.33	-	-	-	-
OG-Net-Small	×	1.20	2.65	80.85	59.56	70.11	49.93	34.87	14.57
OG-Net	×	1.95	4.62	80.94	59.97	71.77	50.81	36.37	15.74

Table 2: We mainly compare three groups of competitive methods with OG-Net on three large-scale person re-id datasets, *i.e.*, Market-1501, DukeMTMC-reID and MSMT-17. We report Rank1(%), mAP(%), the number of model paramters (M) and Multiplier-ACcumulator (G). ‘Pre-trained with ImageNet’ denotes whether the model is trained from scratch or starts from ImageNet pre-trained weight. The first group contains prevailing 2D CNN models. The second group contains the light-weighted CNN models. The third group contains the point-based methods that we re-implemented.

ideal for representation learning. We think it could be solved via the depth estimation devices, such as Kinect [5], or more sophisticated human models in the future. In this paper, we do not solve the 3D human reconstruction problem, but focus on the person re-identification task. Therefore, as a trade-off, we still introduce the 2D background, and project the corresponding pixel to the XY plane (see Figure 4 (c)).

4.2 Qualitative Results

Comparisons to the 2D Space. We compare the results on three kinds of inputs, *i.e.*, 2D input, 3D Visible Part and 3D Visible Part with 2D Background. For a fair comparison, the grid of the 2D input is also transformed to the point cloud format as $(x, y, 0)$, while z is set to 0. We train OG-Net on three kinds of input data with the same hyper-parameters. As shown in Table 1, we observe that the retrieval result of the pure 3D Visible Part input is inferior to that of 2D Image. As discussed in Section 4.1, we speculate that it is due to the lossy 2D-to-3D mapping, which drops several discriminative parts, such as hair, dress, and carrying. In contrast, the 3D Visible Part + 2D Background has achieved superior performance 59.97% mAP to the result of 2D Image (57.28% mAP), which shows that the 3D position information is complementary to 2D color information. The 3D space could ease the matching difficulty and highlight the geometry structure.

Person Re-id Performance. We compare the proposed method with three groups of competitive methods, *i.e.*, prevailing 2D CNN models, light-weight CNN models, and popular point classification models. We note that the model pre-trained on the large-scale datasets, *e.g.*, ImageNet [1], could yield the performance boost. For a fair comparison, most models are trained from scratch with the same optimization objective, *i.e.*, the cross-entropy loss. As shown in Table 2, we can make the following observations:

(1) OG-Net has achieved competitive results of 59.97% mAP, 50.81% mAP and 15.74% mAP on three large-scale benchmarks with limited training parameters 1.95M. The mobile OG-Net-Small with less channel width also achieves a close result.

Method	Pretrained	Duke→Market		Market→Duke	
		R@1	mAP	R@1	mAP
PN-GAN [18]	✓	-	-	29.9	15.8
DG-Net [44]	✓	56.1	26.8	42.6	24.3
DenseNet-121	×	32.7	11.6	11.7	5.0
ResNet-50	×	34.3	13.5	12.1	5.2
ResNet-50	✓	41.2	16.6	21.4	9.9
OG-Net	×	40.0	16.1	26.8	13.8

Table 3: Transfer learning to unseen datasets.

Index	Method	R@1	R@10	mAP
1	No KNN Graph (<i>i.e.</i> , $k=1$)	79.66	95.10	56.06
2	More Neighbors (<i>i.e.</i> , $k=32$)	78.92	95.10	57.23
3	No Last Non-local	80.61	95.34	59.05
4	No SE	80.79	95.25	60.16
5	With short-cut connection	81.21	95.90	59.56
6	Ours	80.94	95.37	59.97

Table 4: Effectiveness of different components.

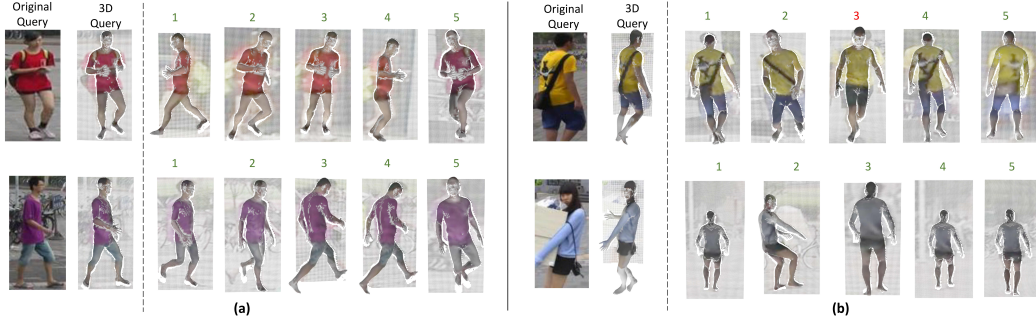


Figure 5: Visualization of Retrieval Results. (a) Given one 3D query, we show the original 2D images and the top-5 retrieval results. (b) We also show two challenging cases, such as occlusion and part detected query. The green index indicates the true-matches, while the red index denotes the false-matches.

(2) Comparing with the point-based methods, such as PointNet++ [16] and DGCNN [30], OG-Net and OG-Net-Small have surpassed this line of works by a clear margin, which validates the effectiveness of the proposed Omni-scale module in capturing neighbor information.

(3) Comparing with light-weight CNN models, *i.e.*, ShuffleNetV2 [39] and MobileNetV2 [20], OG-Net-Small has achieved competitive performance with fewer parameters.

(4) Comparing with prevailing 2D CNN models, *i.e.*, ResNet-50 [6] and DenseNet-121 [8], the proposed OG-Net does not surpass these models. In contrast, we observe that OG-Net is more robust than 2D CNNs, when facing the unseen data. We will discuss this aspect in the following section.

Transferring to Unseen Datasets. To verify the scalability of OG-Net, we train the model on dataset A and directly test the model on dataset B (with no adaptation). We denote the direct transfer learning protocol as $A \rightarrow B$. Two groups of related works are considered. As shown in Table 3, OG-Net is inferior to the GAN-based method, *i.e.*, PN-GAN [18] and DG-Net [44]. It is because the GAN-based methods introduce extra synthetic data, which regularizes the training process. In contrast, OG-Net is superior to ResNet-50 / DenseNet-121 and is competitive to the ResNet-50 pre-trained on ImageNet. The results suggest that the proposed method has the potential to adapt one new re-id dataset of unseen camera networks.

4.3 Quantitative Results

Visualization of Retrieval Results. As shown in Figure 5, we provide the original query, the corresponding 3D query and the top-5 retrieved candidates. Two different cases are studied. One is the typical case that the 3D human reconstruction is relatively good. OG-Net could successfully retrieve the true-matches (see Figure 5 (a)). On the other hand, we also show two challenging cases, including part detection and occlusion. Thanks to the prior knowledge of the human geometry structure, OG-Net can still provide reasonable retrieval results (see Figure 5 (b)).

5 Further Analysis and Discussions

Effect of Different Components. In this section, we intend to study the mechanism of the Omni-scale Module. First, we compare the OG-Net without KNN Graph, *i.e.*, $k = 1$. For a fair comparison, we apply one linear layer to replace the dynamic graph convolution. As shown in Table 4(1), the

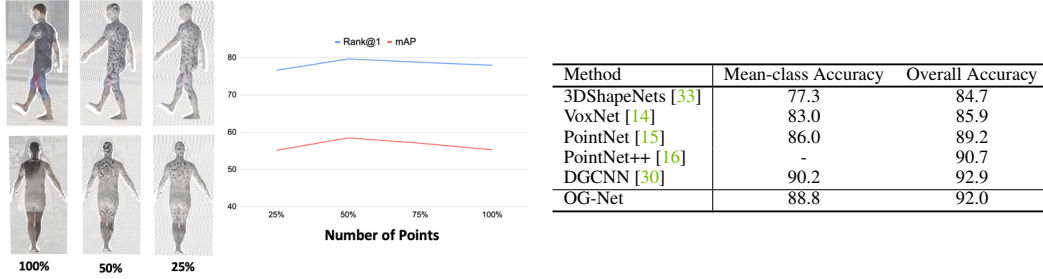


Figure 6: Results of our model on point density.

Table 5: Classification results on ModelNet.

performance of OG-Net without leveraging the KNN neighbor information drops to 54.35 mAP. The result suggests that the dynamic graph captures effective local information, which could not be replaced by pre-point function, *e.g.*, linear layer. On the other hand, if we include too many neighbors, *e.g.*, $k = 32$, the model loses the discriminative feature of local patterns, thus compromising the retrieval performance as well (see Table 4(2)). Next, we intend to verify the effectiveness of the last non-local graph. The last graph is built on the k -nearest neighbor of the appearance feature. (In practice, we append the 3-channel position to the appearance feature for building the graph, which prevents duplicate nodes with the same node attribute in the graph.) For a fair comparison, we replace the last non-local graph with the graph based on 3D position only. As shown in Table 4(3) and (6), OG-Net with the last non-local block has surpassed the model with position graph +0.92% mAP, indicating that the last non-local graph provides effective long-distance attention. Finally, we study two alternative components, *i.e.*, SE block and short-cut connection. By default, Omni-scale Module deploys SE block but does not add the short-cut connection. As shown in Table 4(4,5), we find that SE Block and the short-cut connections do not provide significant improvement or performance drop. We speculate that it might be due to the model depth. OG-Net is relatively shallow with four Omni-scale blocks, and could not reflect the superiority of SE-block and the short-cut connection.

Effect of the Number of Input Points. Our model is trained with 50% points, *i.e.*, 4096, and thus the best performance is achieved with 50% points remaining. In practice, different depth estimation devices may provide different scan point density. To verify the robustness of the proposed OG-Net on point density, we synthesize the data similar to that in Figure 6 (left) and conduct the inference. When 25% points remain, OG-Net still could arrive at 76.60% Rank@1 and 55.17% mAP. When 100% points are used, OG-Net arrives at 77.94% Rank@1 and 55.30% mAP. It is because too low/high density impacts the distribution of the k -nearest neighbors, compromising the retrieval performance. Despite the density changes, the relative performance drop is small. The result verifies OG-Net is robust to different point density (see Figure 6 (right)).

Evaluation of Point Cloud Classification Task. We also evaluate the proposed OG-Net on the traditional point cloud classification benchmark, *i.e.*, ModelNet [33]. Note that ModelNet does not provide RGB information. To verify the effectiveness of OG-Net, we duplicate the xyz input as the appearance input to train OG-Net. The number of input points is 1024. As shown in Table 5, we compare with prevailing models in terms of mean-class accuracy and overall accuracy. Although OG-Net is not designed for cloud point classification task, OG-Net also achieves a competitive result.

6 Conclusion

In this work, we provide an early attempt to learn the pedestrian representation in the 3D space. Our result suggests that 3D geometry information is complementary to the original 2D appearance. The proposed OG-Net takes the advantage of the 3D prior knowledge, yielding competitive performance with limited parameters. We hope this work can pave the way for future studies in 3D person re-id. We will continue working on this task and solving the potential drawbacks in two directions: 1. 2D images are usually resized and compressed in most person re-id datasets, compromising the body shape, *e.g.*, height. We may consider collecting a new 3D dataset in the future. 2. Besides, we will apply the proposed approach to other potential fields, *e.g.*, objectives with a rigid structure like vehicle [28] and product [32].

Broader Impact

This work can be attributed to 1) the increasing demand for public safety and 2) the widespread camera networks in theme parks, university campuses, and streets. For instance, it is usually time-consuming to find a lost child across cameras in the theme park. This work could reduce the time cost and save human resources, providing a robust prediction.

References

- [1] J. Deng, W. Dong, R. Socher, L.-J. Li, K. Li, and L. Fei-Fei. Imagenet: A large-scale hierarchical image database. In *CVPR*, 2009. 6
- [2] C. Eom and B. Ham. Learning disentangled representation for robust person re-identification. In *NeurIPS*, 2019. 2
- [3] Y. Ge, Z. Li, H. Zhao, G. Yin, S. Yi, X. Wang, and H. Li. Fd-gan: Pose-guided feature distilling gan for robust person re-identification. In *NeurIPS*, 2018. 2
- [4] W. Hamilton, Z. Ying, and J. Leskovec. Inductive representation learning on large graphs. In *NeurIPS*, 2017. 5
- [5] J. Han, L. Shao, D. Xu, and J. Shotton. Enhanced computer vision with microsoft kinect sensor: A review. *IEEE transactions on cybernetics*, 43(5):1318–1334, 2013. 6
- [6] K. He, X. Zhang, S. Ren, and J. Sun. Deep residual learning for image recognition. In *CVPR*, 2016. 4, 6, 7
- [7] J. Hu, L. Shen, and G. Sun. Squeeze-and-excitation networks. In *Proceedings of the IEEE conference on computer vision and pattern recognition*, pages 7132–7141, 2018. 4
- [8] G. Huang, Z. Liu, L. V. D. Maaten, and K. Q. Weinberger. Densely connected convolutional networks. In *CVPR*, 2017. 6, 7
- [9] M. M. Kalayeh, E. Basaran, M. Gökmen, M. E. Kamasak, and M. Shah. Human semantic parsing for person re-identification. In *CVPR*, 2018. 2
- [10] A. Kanazawa, M. J. Black, D. W. Jacobs, and J. Malik. End-to-end recovery of human shape and pose. In *CVPR*, 2018. 2, 3
- [11] D. P. Kingma and J. Ba. Adam: A method for stochastic optimization. *arXiv preprint arXiv:1412.6980*, 2014. 5
- [12] J. Liu, B. Ni, Y. Yan, P. Zhou, S. Cheng, and J. Hu. Pose transferrable person re-identification. In *CVPR*, 2018. 2
- [13] I. Loshchilov and F. Hutter. Sgdr: Stochastic gradient descent with warm restarts. *ICLR*, 2017. 5
- [14] D. Maturana and S. Scherer. Voxnet: A 3d convolutional neural network for real-time object recognition. In *2015 IEEE/RSJ International Conference on Intelligent Robots and Systems (IROS)*, pages 922–928. IEEE, 2015. 8
- [15] C. R. Qi, H. Su, K. Mo, and L. J. Guibas. Pointnet: Deep learning on point sets for 3d classification and segmentation. In *CVPR*, 2017. 2, 5, 8
- [16] C. R. Qi, L. Yi, H. Su, and L. J. Guibas. Pointnet++: Deep hierarchical feature learning on point sets in a metric space. In *NeurIPS*, 2017. 2, 4, 5, 6, 7, 8
- [17] X. Qian, Y. Fu, Y.-G. Jiang, T. Xiang, and X. Xue. Multi-scale deep learning architectures for person re-identification. In *ICCV*, 2017. 2
- [18] X. Qian, Y. Fu, T. Xiang, W. Wang, J. Qiu, Y. Wu, Y.-G. Jiang, and X. Xue. Pose-normalized image generation for person re-identification. In *ECCV*, 2018. 2, 7
- [19] E. Ristani, F. Solera, R. Zou, R. Cucchiara, and C. Tomasi. Performance measures and a data set for multi-target, multi-camera tracking. In *ECCV*, 2016. 5
- [20] M. Sandler, A. Howard, M. Zhu, A. Zhmoginov, and L.-C. Chen. Mobilenetv2: Inverted residuals and linear bottlenecks. In *CVPR*, 2018. 6, 7
- [21] F. Scarselli, M. Gori, A. C. Tsoi, M. Hagenbuchner, and G. Monfardini. The graph neural network model. *IEEE Transactions on Neural Networks*, 20(1):61–80, 2008. 3
- [22] C. Su, J. Li, S. Zhang, J. Xing, W. Gao, and Q. Tian. Pose-driven deep convolutional model for person re-identification. In *ICCV*, 2017. 2
- [23] Y. Suh, J. Wang, S. Tang, T. Mei, and K. Mu Lee. Part-aligned bilinear representations for person re-identification. In *ECCV*, 2018. 2
- [24] X. Sun and L. Zheng. Dissecting person re-identification from the viewpoint of viewpoint. In *CVPR*, 2019. 1, 2
- [25] Y. Sun, L. Zheng, Y. Yang, Q. Tian, and S. Wang. Beyond part models: Person retrieval with refined part pooling. *ECCV*, 2018. 2
- [26] C. Szegedy, S. Ioffe, V. Vanhoucke, and A. A. Alemi. Inception-v4, inception-resnet and the impact of residual connections on learning. In *AAAI*, 2017. 4

- [27] Z. Tang, M. Naphade, S. Birchfield, J. Tremblay, W. Hodge, R. Kumar, S. Wang, and X. Yang. Pamtri: Pose-aware multi-task learning for vehicle re-identification using highly randomized synthetic data. In *ICCV*, 2019. [2](#)
- [28] Z. Tang, M. Naphade, M.-Y. Liu, X. Yang, S. Birchfield, S. Wang, R. Kumar, D. Anastasiu, and J.-N. Hwang. Cityflow: A city-scale benchmark for multi-target multi-camera vehicle tracking and re-identification. In *CVPR*, 2019. [8](#)
- [29] X. Wang, R. Girshick, A. Gupta, and K. He. Non-local neural networks. In *CVPR*, 2018. [3](#)
- [30] Y. Wang, Y. Sun, Z. Liu, S. E. Sarma, M. M. Bronstein, and J. M. Solomon. Dynamic graph cnn for learning on point clouds. *ACM Transactions on Graphics (TOG)*, 38(5):1–12, 2019. [1](#), [3](#), [4](#), [5](#), [6](#), [7](#), [8](#)
- [31] L. Wei, S. Zhang, W. Gao, and Q. Tian. Person transfer gan to bridge domain gap for person re-identification. In *CVPR*, 2018. [5](#)
- [32] X.-S. Wei, Q. Cui, L. Yang, P. Wang, and L. Liu. Rpc: A large-scale retail product checkout dataset. *arXiv:1901.07249*, 2019. [8](#)
- [33] Z. Wu, S. Song, A. Khosla, F. Yu, L. Zhang, X. Tang, and J. Xiao. 3d shapenets: A deep representation for volumetric shapes. In *Proceedings of the IEEE conference on computer vision and pattern recognition*, pages 1912–1920, 2015. [8](#)
- [34] K. Xu, W. Hu, J. Leskovec, and S. Jegelka. How powerful are graph neural networks? *arXiv preprint arXiv:1810.00826*, 2018. [5](#)
- [35] Y. Yang, C. Feng, Y. Shen, and D. Tian. Foldingnet: Point cloud auto-encoder via deep grid deformation. In *CVPR*, 2018. [5](#)
- [36] Y. Yao, L. Zheng, X. Yang, M. Naphade, and T. Gedeon. Simulating content consistent vehicle datasets with attribute descent. *arXiv:1912.08855*, 2019. [2](#)
- [37] H. Zhang, I. Goodfellow, D. Metaxas, and A. Odena. Self-attention generative adversarial networks. *arXiv:1805.08318*, 2018. [3](#)
- [38] X. Zhang, H. Luo, X. Fan, W. Xiang, Y. Sun, Q. Xiao, W. Jiang, C. Zhang, and J. Sun. Alignedreid: Surpassing human-level performance in person re-identification. *arXiv:1711.08184*, 2017. [1](#)
- [39] X. Zhang, X. Zhou, M. Lin, and J. Sun. Shufflenet: An extremely efficient convolutional neural network for mobile devices. In *CVPR*, 2018. [6](#), [7](#)
- [40] F. Zheng, C. Deng, X. Sun, X. Jiang, X. Guo, Z. Yu, F. Huang, and R. Ji. Pyramidal person re-identification via multi-loss dynamic training. In *CVPR*, 2019. [2](#)
- [41] L. Zheng, Y. Huang, H. Lu, and Y. Yang. Pose-invariant embedding for deep person re-identification. *IEEE Transactions on Image Processing*, 28(9):4500–4509, 2019. [2](#)
- [42] L. Zheng, L. Shen, L. Tian, S. Wang, J. Wang, and Q. Tian. Scalable person re-identification: A benchmark. In *ICCV*, 2015. [5](#)
- [43] L. Zheng, Y. Yang, and A. G. Hauptmann. Person re-identification: Past, present and future. *arXiv:1610.02984*, 2016. [1](#)
- [44] Z. Zheng, X. Yang, Z. Yu, L. Zheng, Y. Yang, and J. Kautz. Joint discriminative and generative learning for person re-identification. In *CVPR*, 2019. [1](#), [2](#), [7](#)
- [45] Z. Zheng, L. Zheng, and Y. Yang. Unlabeled samples generated by gan improve the person re-identification baseline in vitro. In *ICCV*, 2017. [2](#), [5](#)
- [46] Z. Zheng, L. Zheng, and Y. Yang. A discriminatively learned cnn embedding for person reidentification. *ACM Transactions on Multimedia Computing, Communications, and Applications (TOMM)*, 14(1):13, 2018. [1](#)
- [47] Z. Zheng, L. Zheng, and Y. Yang. Pedestrian alignment network for large-scale person re-identification. *IEEE Transactions on Circuits and Systems for Video Technology*, 2018. [2](#)
- [48] Z. Zhong, L. Zheng, Z. Zheng, S. Li, and Y. Yang. Camera style adaptation for person re-identification. In *CVPR*, 2018. [2](#)
- [49] K. Zhou, Y. Yang, A. Cavallaro, and T. Xiang. Omni-scale feature learning for person re-identification. In *ICCV*, 2019. [2](#)